Journal of the Physical Society of Japan
Vol. 69, No. 5, May, 2000, pp. 1374-1383

Absolute Total and Partial Cross-Sections for Ionization of Ba and Eu Atoms by Electron Impact

Shuichi YAGI and Tetsuo NAGATA

Department of Physics, Meisei University, Tokyo 191-8506

(Received September 16, 1999)

Experimental apparatus and procedure for measurements of absolute total (apparent and counting) and relative partial cross sections for ionization of atoms by electron impact are described in some detail, and results on Ba and Eu atom are reported. A crossed electron-atom beam ion source combined with a 60° sector mass analyzer has been used to measure the partial cross sections. For the measurement of the absolute total cross sections, another type of crossed electron-atom beam arrangement combined with a time-of-flight (TOF) velocity measurements of target atoms has been used. The absolute cross sections have been determined with experimental accuracy of ±23%, and have been used to calibrate the partial cross-sections. The results of Ba atom agree well with previously reported results. The Eu^+ cross section curve shows remarkable peak structure near the $4f$ ionization thresholds, probably attributed to the resonance excitation of $4f^6 6s^2 nl$ aoutoionization states via temporal negative-ion formation.

KEYWORDS: cross section, electron impact, ionization, lanthanide, barium, europium

§1. Introduction

Ionization of atoms by electron impact has long been one of the basic subjects in atomic physics. A great number of experimental and theoretical studies has been reported on inert-gas atoms, and also has been reported on alkali and alkaline-earth atoms, which are rather easily be vaporized. Studies of metals with high boiling point are relatively few because of the experimental difficulties. We can make reference to excellent reviews,[1, 2] data books[3, 4] and text books[5, 6] on previous experimental and theoretical studies on this subject.

In a present series of experimental studies, we have investigated electron impact ionization of eight lanthanide elements: Ce, Nd, Sm, Eu, Gd, Dy, Er and Yb. We also measured the Ba atoms, for which previous data are available[7-9] to confirm the reliability of our apparatus. On the electron-impact ionization of lanthanide atoms, we find in the literature only one experiment by Shimon *et al.*[10] They measured the cross sections of single to triple ionization of Sm, Eu, Tm, and Yb atoms at electron energies up to 200 eV.

In a present paper, we study the lanthanides on the following three motivations. First, when reviewing the experimental data on concerning the electron impact ionization of atoms ranging from hydrogen to uranium, we hardly find the data of $4f$ and $5f$ transition-metal atoms. Studies of those atomic species are therefore highly needed to complete our knowledge on the electron impact phenomena in atoms. Second, a lanthanide atom has a $4f$ open subshell, which undergoes a strong correlation with the $5d$ subshell. In the case of photon impact ionizations, we may observe the prominent $4d$-$(4, \varepsilon)f$ giant resonances realized by the $4f$ orbital collapse.[11, 12] For the electron impact ionizations, we do not have much experimental evidence of such the giant resonances. It is interesting to observe the behavior of $4f$ subshell orbital collapse and of the $4f$–$5d$ orbital correlations under the incidence of an extra electron by electron impact on atoms. Third, the elements that have been rendered for future studies generally require high temperature for vaporization like the most transition elements, or they are extremely reactive like VIB and VIIB elements. Serious difficulties are present in the absolute measurement on such the elements; they are the difficulties in vaporizing the metallic sample in vacuum and in determining the target-atom density. It is very important and highly needed to establish an experimental technique to measure the ionization cross sections of those elements.

Recent developments of experimental technique have enabled us to perform precision measurements on the scattering cross sections and to treat various target elements. Wetzel *et al.*[13] and Freurd *et al.*[14] used a crossed-electron-fast-neutral beam method, and measured successively the absolute partial cross sections for 27 kinds of atoms including VIB and VIIB reactive elements. One particular difficulty in this method could be, however, the existence of excited metastable species in the fast neutral beam. More recent experiment on electron impact ionization reported by Strub *et al.*[15] is highly progressive. They measured the absolute partial cross sections for formation of Ar^{q+} ($q = 1$–4) ions with estimated uncertainties of 3.0–8.0% at 200 eV using a simple apparatus design. However, the apparatus is designed for gas-phase targets only.

One of the most difficult problems in the cross-section measurements of metallic atoms is the determination of target-atom number density. It requires the knowledge of a flux and an average velocity of atoms passing through the collision region. The most accepted method for determining the flux is the accumulation of atoms on a cold surface. In this method, the accumulation coefficient (or

sticking probability) must be well known. In a present study, we used an atomic beam sensor made of a quartz crystal resonator (hereafter, called quartz crystal sensor. See §2.3.2) instead of the cold trap. For the determination of average atom velocity, we used the time-of-flight technique, because it was difficult to measure correctly the temperature of the present high-temperature oven.

Except the beam monitoring technique mentioned above, we used a rather traditional method in the present series of studies; that is, measurement of the relative partial cross sections using a magnetic deflection mass spectrometer and that of the absolute total cross sections using a crossed-beam apparatus. The relative partial cross sections for single to triple or quadruple ionization have been measured in the impact energy range from the single ionization threshold to 900 eV. The absolute total cross sections have been measured at electron impact energies 400, 600 and 900 eV, and the result have been used to calibrate the partial cross sections.

In this paper, the experimental apparatus and procedure are described in detail, and the results on Ba and Eu atoms are reported with emphasis on Eu atom. The results on the other lanthanide atoms will be reported in a forthcoming paper.

§2. Experiment

2.1 General

The vacuum chambers and the related evacuation system of the present apparatus are basically made of stainless steel. In the construction of all the assemblies set in the vacuum chambers, we avoided the use of spot welding to prevent the parts from magnetization. The main chamber, in which the atoms were ionized, was evacuated with a 200 ℓ/s turbo-molecular pump. The background pressure in the chamber was lower than 1.5×10^{-4} Pa.

It would be appropriate here to make clear the definition of various cross sections. The absolute total ionization cross section σ_T is defined as

$$\sigma_T = \sum_{q=1} q\sigma_{q+}, \tag{1}$$

where σ_{q+} is the partial cross section for the formation of M^{q+} ion from atomic species M. The absolute cross section σ_T (sometimes called apparent cross section) can be determined directly by measuring total ion current from a precisely defined collision volume in an appropriately designed experimental assembly. Sum of the partial cross sections

$$\sigma_c = \sum_{q=1} \sigma_{q+} \tag{2}$$

is another important total cross section, and is sometimes called "counting" cross section.[2)] When partial cross sections σ_{q+} are measured absolutely, the absolute total and counting cross sections can be obtained using relation eqs. (1) and (2), respectively.[13-15)] When collecting a constant part of the M^{q+} ions produced in the collision region using a mass spectrometer, and measuring its intensity with changing the electron energy, we obtain relative partial cross sections. These are denoted by σ^r_{q+} in this paper. We can calibrate σ^r_{q+} to obtain σ_{q+} if absolute total cross section σ_T and the charge-state distribution at a given electron energy are available.

2.2 Set up for the relative partial cross-section measurement

Figure 1 shows the experimental arrangement for the measurement of partial cross sections. It is basically a 60° sector mass spectrometer. The ions formed in the ion source are accelerated and focused into a beam electrostatically, mass analyzed, and then detected by a suppressed Faraday cup or a secondary-electron multiplier.

2.2.1 Details of the ion source

In order to obtain reliable partial cross-section functions, the ion source must be well characterized. Of most important is to ensure that a constant fraction from the ions produced in the ionization cell is detected independent of the m/q ratio, the electron impact energy and the ion extraction voltage. The insertion in Fig. 1 displays the details of the ion source. This is essentially a Nier-type ion source, and the extraction of ions is based on the penetrating field method.[2)] The entrance window of 6.0 mm × 8.0 mm for the atomic beam is stretched across by tungsten net of 8 mesh (wires of 0.15 mm in diameter).

The collimator of the electron beam is a cylinder with entrance and exit apertures of 3.0 mm in diameter. No lens system to collimate the electron beam was used because, in preliminary measurements, the shape of the partial cross-section curves was found to alter by conditions of this lens system. No magnetic field was used to collimate the electron beam. The electron collector C is

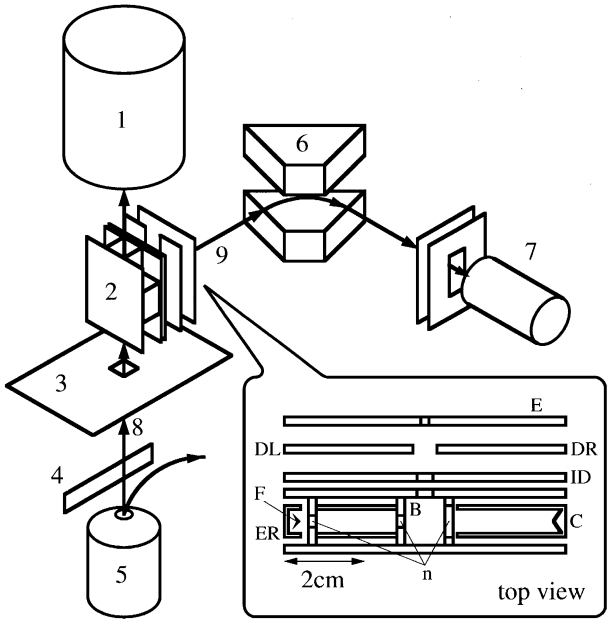

Fig. 1. Experimental arrangement for the measurement of relative partial cross section. 1: Cold trap. 2: Electron impact type ion source. 3: Radiation-shielding plate. 4: Charged-particle deflector. 5: Oven. 6: 60° sector magnet. 7: Secondary-electron multiplier or Faraday cup. 8: Neutral metal-atom beam. 9: Ion beam. The insertion is the details of the ion source. B: Ionization box. ID: Ion drawer electrode. DR and DL: Ion deflectors. E: Earth electrode. F: Electron emitter (tungsten filament). ER: Electron repeller electrode. C: Electron collector. n: Tungsten net.

kept at a voltage by 10 V higher than that of B.

The voltage of the ion extractor ID with respect to that of B was kept as low as possible, because there is a possibility that the electric field penetrating into the ionization box modifies the real cross-section curves. The energy spread of incident electron beam is estimated to be 1.2 eV. This value is based on the thermal spread (0.4 eV) and the potential difference (0.8 V) along the effective length of the tungsten wire.

2.2.2 Metal vapor oven

In the present study, the temperature 1000–2000 K is required to vaporize the metal samples. One of efficient high-temperature ovens is of the electron bombardment type, as used in this study. The outline of the oven and related electronics are shown schematically in Fig. 2. The reservoir is bombarded by energetic (0.5–2.6 keV) electrons from three tungsten wires of 0.3 mm in diameter. Outside the wires, cylindrical radiation shields are placed triply. A ring electrode is fixed on the top of the innermost cylinder. From this ring, the tungsten wires and a disc electrode are hang down. The disc is not fixed to avoid the bending of wires when they are heated. On the top of the oven, a cap with a hole of 10 mm in diameter is placed. The chamber is surrounded by a coiled water-cooling pipe. The reservoir, the inner most radiation shield, the ring electrode and the disc electrode are made of tantalum, and others are made of stainless steel. Material of the crucible was carbon, tantalum or stainless steel, depending on the metal sample used.[16] One operation of the oven lasted about two days.

2.3 Set up for the absolute total cross-section measurement

Figure 3 displays the entire arrangement in this absolute measurement. The entire system in vacuum can be divided into two sections, the ionization section, and the target-atom monitoring section. The elements contained are, in the order from bottom to top, the metal vapor oven, a shielding plate with a shutter, a crossed electron-atom beam assembly, a pulsed electron gun, a drift tube, a channeltron, the quartz crystal sensor and a cold trap. The metal vapor oven used is the same as that in the measurement of the relative partial cross-sections.

2.3.1 Details of the crossed electron-atom beam assembly

Figure 4 displays the crossed electron-atom beam assembly for measurement of absolute intensity of ionizing electrons I_e and that of resulting ions I_i [see eq. (4) in §3.2]. The entrance and exit windows for the atomic beam and the window of ID for ion collection are stretched across by tungsten grids of 1.9 mm spac-

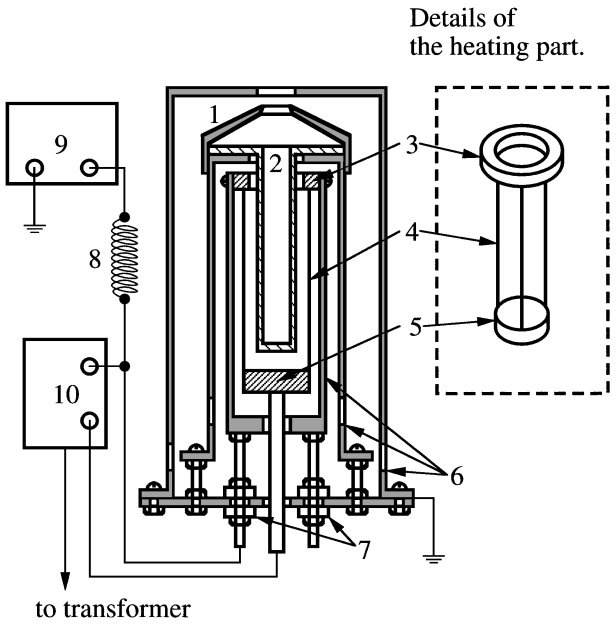

Fig. 2. Details of the metal vapor oven. 1: Cap. 2: Reservoir. 3: Ring electrode. 4: Tungsten wire. 5: Disc electrode. 6: Cylindrical radiation shield. 7: Ceramic insulator. 8: Self-induction coil. 9: High voltage power supply (for electron accelation). 10: Power supply (for heating tungsten wire).

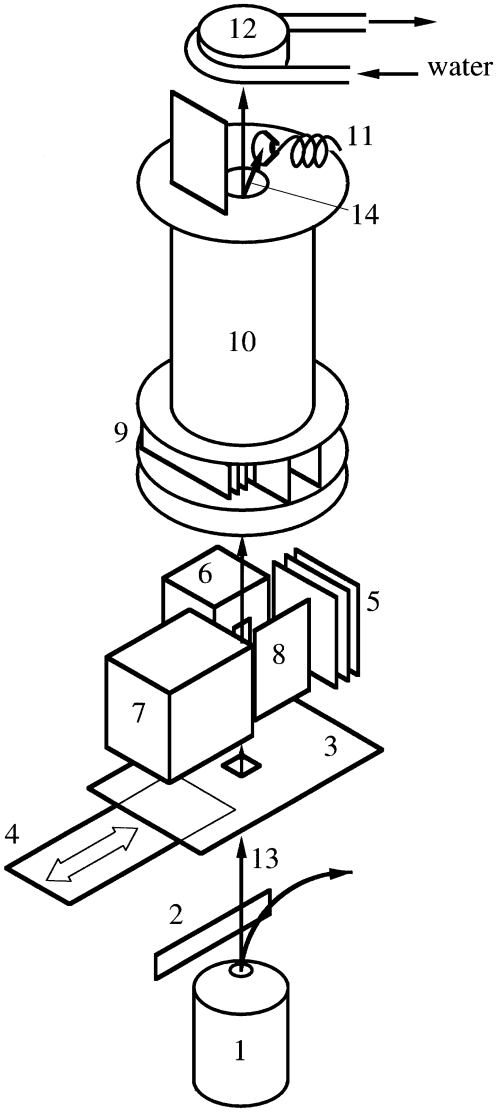

Fig. 3. Experimental arrangement for the absolute total cross-section measurement. 1: Metal vapor oven. 2: Charged-particle deflector. 3: Shielding plate. 4: Shutter. 5: Electron gun. 6: Ion collector. 7: Electron collector. 8: Ion repeller. 9: Pulsed electron gun. 10: Drift tube. 11: Channeltron. 12: Quartz crystal sensor. 13: Neutral metal-atom beam. 14: Pulsed ion beam. A cold trap is set above the crystal sensor.

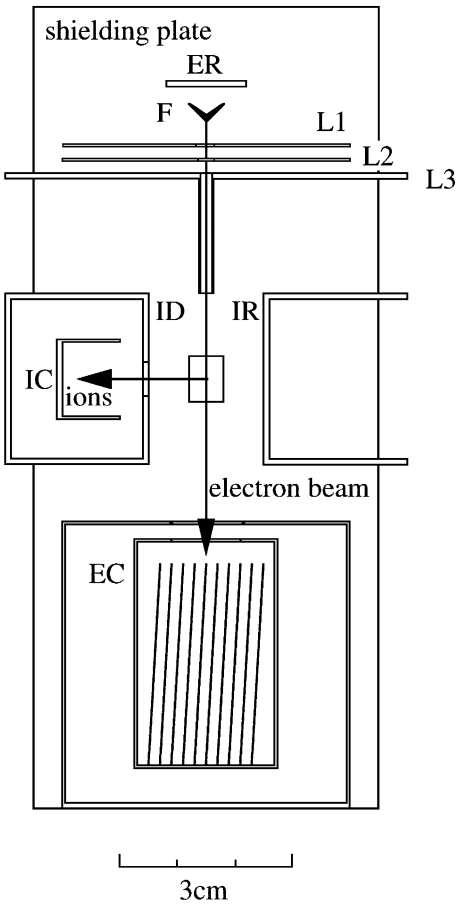

Fig. 4. Details of the ionization region for the absolute total cross-section measurement (top view). IR: Ion repeller. ID: Ion drawer. F: Electron emitter (tungsten filament). ER: Electron repeller. EC: Electron collector. L1, L2 and L3: Electron-beam lens system.

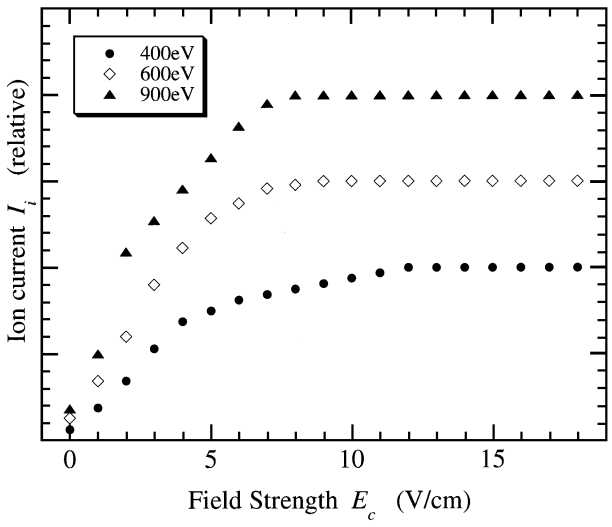

Fig. 5. The intensity of collector ion current I_i as a function of the field strength E_c.

ing. In this experiment, the collision center (the center of electron-atom interaction region) was kept at the ground potential. Voltages on the surrounding electrodes were applied appropriately with respect to this collision-center potential.

The design of the electron and ion collectors is very important because I_e and I_i are the direct quantities in the determination of σ_T. The electron collector EC is a deep open box, of which inside is partitioned into a number of small deep and open cells with very thin plates. In addition, the voltage of EC is kept at +36 V, preventing almost perfectly the secondary electrons from escaping.

The electrodes IR and ID are placed symmetrically with respect to the electron beam, and are used to provide a weak and uniform electric-field to push the produced ions into the rectangular opening (5.8 mm × 15.0 mm) of ID, the shorter being in the electron-beam direction. It is assumed that only ions which are produced in the region perpendicular to the opening enter the ion collector.

One of the important factors for accurate measurement of I_i is the effect of the thermal motion of target atoms. The velocity of target atoms amounts to 450–650 m/s, depending on the target used and the oven temperature. A simple calculation shows that the produced ions travel 1.1–1.4 mm in the direction of the atomic beam until the ion reaches the ID. For this reason, the openings for ion collection of ID and IC were lengthened in the vertical atomic-beam direction. Under this geometrical condition, we measured the ion current changing the field strength E_c at a fixed bias (1 V) between ID and IC. The results are shown in Fig. 5 for the electron impact energies 400, 600, and 900 eV. We see that the ion current saturates for $E_c > 12$ V/cm. On the basis of this result, the voltage of the ion collector was kept 1.0 V lower than that of ID, and the field strength E_c was fixed at 15 V/cm.

In the absolute total cross-section measurement as in the present method, it is important to discriminate the ions under study from background ions. A shutter allows us to do this discrimination. The purity of metal samples used was better than 99.9%. Concerning the contamination of molecular ions in the atomic beam, we observed a small amount at the beginning of the heating in the partial cross section measurement, but it reduced to a negligible level after the several hours of degassing.

2.3.2 Monitoring of atomic-beam

The upper half (No. 9–No. 12) of Fig. 3 is the assembly used to determine the target-atom density N. The determination of N requires the average velocity $\langle\nu\rangle_{\rm av}$ of target atoms as well as the accumulation rate T and the accumulation coefficient η of atoms on the surface of the quartz crystal sensor (see eq. (4) in §3.2). The average velocity $\langle\nu\rangle_{\rm av}$ was determined by a time-of-flight (TOF) technique using the pulsed electron gun operated with a pulse generator. The pulsed ion beam thus formed drifts in the field-free TOF tube of 16.0 cm, passes through its exit hole, and then is accelerated into the head of channeltron by its strong electrostatic field. The pulse signals from the channeltron, after passing through an amplifier and a SCA module, enter a digital storagescope triggered by pulses from the pulse generator, and recorded as a time spectrum.

A part of neutral atoms, after passing through the TOF region, reach the quartz crystal sensor. The controller of the sensor indicates the accumulation rate of target atoms on the sensor surface. The cooled water runs around the sensor head. So that the accumulation of target atoms on the crystal surface is not influenced by the radiation from the oven (see §4.2.6).

§3. Determination of Cross Sections

3.1 Relative partial cross-section

The partial ionization cross-section σ_{q+} is given by

$$\sigma_{q+} = C \cdot \frac{I_i}{I_e}, \ (q = 1, 2, 3, 4), \tag{3}$$

where I_e is the electron current in the ion source, I_i is the ion current, and C is a constant. The constant C contains parameters such as the target-atom density, the effective collision length, and the fraction of ions detected by the ion collector. The constancy of C is ensured if these parameters are kept constant regardless of the electron impact energy and the ionic charge. The cross-section σ_{q+} will be absolute if C is known correctly. Because C was in fact unknown at the stage of measurement using the mass selector, we calculated σ_{q+} assuming C at a proper value. We call it the relative partial cross-section and denote as σ^r_{q+}.

Then, the determination of the partial cross sections σ_{q+} consists of measuring the relative cross-section curves σ^r_{q+} as well as the charge-state distribution, and calibrating these relative curves to absolute scale using the results of the charge-state distribution and the absolute total cross section σ_T.

The measurement of σ^r_{q+} was done at electron-energy intervals of 0.5–100 eV from the ionization threshold to 900 eV. The energy interval was taken smaller near the threshold. The relative measurement was repeated several times for a given ionic species M^{q+}. When the ion-beam intensity was too weak to be measured directly with a dc electrometer, the electron multiplier was used in dc mode.

The partial cross-section measurement on one element was made repeatedly and extended typically over 2 days. During or after this partial measurement, we measured mass spectra precisely at electron energy 400 eV using the suppressed Faraday cup to determine reliable charge-state distribution. In this measurement, the density of target atoms was increased to about ten times that when the partial curves were measured. This value was a level at which the charge-state distribution could be measured easily by dc amplifier but secondary effect was still negligible.

3.2 Absolute total cross-sections

When a single collision condition applies, the absolute total (counting) cross-section σ_c is given by

$$\sigma_c = \frac{I_i}{I_e \cdot N \cdot L \cdot \langle q \rangle_{\rm av}}, \tag{4}$$

using previously introduced I_i, the total ion current, I_e, the electron current, and N, the target atom density in the ionization region, and using further on the effective collision length L and $\langle q \rangle_{\rm av}$ the average ion charge $\langle q \rangle_{\rm av}$, which can be calculated from the charge-state distribution, as

$$\langle q \rangle_{\rm av} = \sum_q q \cdot f_q, \tag{5}$$

where q is the ionic charge and f_q is the fraction of ions with charge q. If $\langle q \rangle_{\rm av}$ in (4) is replaced by unity, we obtain absolute total (apparent) cross section σ_T.

The target atom density N is given by

$$N = \frac{T \cdot \rho}{M \cdot \eta \cdot \langle \nu \rangle_{\rm av}} \cdot \frac{I_C}{I_S}, \tag{6}$$

where T is the accumulation rate of target atoms on the surface of the crystal sensor, ρ is the density of a given element in solid phase, I_S and I_C are the intensities of the atomic beam at the sensor and the collision center, η is the accumulation coefficient (sticking probability) of atoms on the sensor surface, and M is the mass of target atom. It is assumed that $\eta = 1$ for both Ba and Eu atoms (see §4.2.6). The number density N is often evaluated assuming the isotropic divergence of the atoms from the source. However, this may not apply in the present case, because the diameter (10 mm) of the oven aperture is not always negligible in comparison with the distance (45 mm) between the aperture and the collision center. Consequently, we measured directly the intensity ratio I_C/I_S by using a couple of surface ionization detectors. We obtained $I_C/I_S = 99.5$ for both Ba and Eu with estimated uncertainty of 7% (see, §4.2.5).

The absolute measurement was done at electron impact energies 400, 600 and 900 eV. The experimental procedure was as follows. An enough time was taken until the ion beam intensity reached an equilibrium. The intensity of ions I_i was recorded with the shutter opened and closed. At the same tame, the accumulation rate T and the electron current I_e were monitored. When the TOF velocity measurement of the target atoms was done, the electron beam in the ionization region was switched off, and the pulsed electron gun was operated instead. The electron beam was pulsed with square pulse from the pulse generator at a frequency 500 Hz (period 2 ms). The width of the square pulse was 30.0 μs and the height of it was 20.0 V. The ion signals were stored typically for 4096 pulses as the time spectrum. We calculated analytically the average transit time $\langle t \rangle_{\rm av}$, and then obtained the average velocity $\langle v \rangle_{\rm av}$. The energy of the electrons in the pulsed electron gun was sufficiently lowered (10–15 eV) so that the target atoms were ionized effectively whereas the background molecules were not.

§4. Results and Discussion

4.1 Ba and Eu atoms

Before making measurement on rare-earth atoms, we made performance tests of the experimental apparatus with Ar and Ba atoms for which previous reliable experimental data are available. For the σ^r_+ and σ^r_{2+} curves of Ar atom, we obtained results which agreed fairly well with published results.[4] Agreement in the Ba results was also substantially good in both partial cross-section curves and absolute cross-section values. Here, we show

the Ba results as examples.

In Fig. 6, the present partial cross-sections obtained on Ba atom are compared with the results of Okudaira.[17] We see that σ_+ and σ_{3+} curves are well reproduced, but σ_{2+} curve is not near the threshold. The structure of the present Ba^+ curve appearing around 10–20 eV is close to his result. Also, the structure of the Ba^{3+} curves due to autoionization near the triple ionization threshold agrees well each other.

Figure 7 shows the result of the present measurement of σ_T on Ba atom (closed circles). Each data point is an average of three to five determinations, and the error bar includes systematic errors only. The standard deviations were from 2.7 to 3.0% of the measured values.

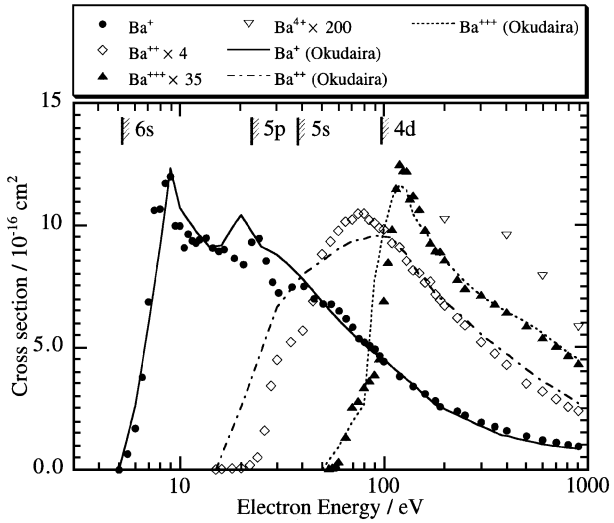

Fig. 6. The partial cross sections for formation of Ba^{n+} ($n = 1$, 2, 3, 4) as a function of electron energy. Note that double, triple and quadruple ionization data are scaled up by 4, 35, 150 times, respectively. The experimental results reported by Okudaira[17] are shown by solid, dashed and dotted curves. His lines are normalized to the present curves. The vertical lines on top show ionization threshold of each subshell.

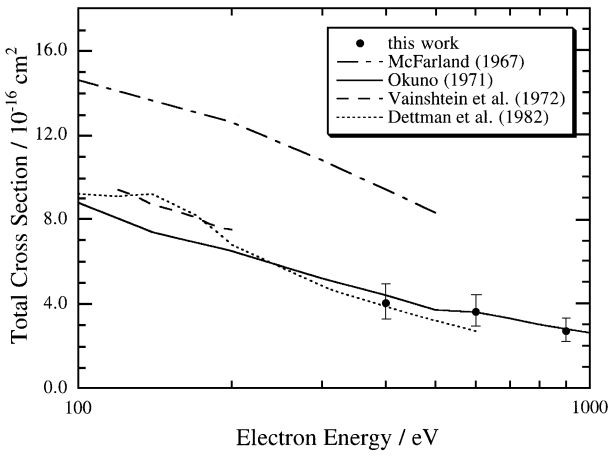

Fig. 7. The absolute total cross-section of Ba as a function of electron energy. The error bars include systematic errors only. Also shown are the experimental results by McFaland (chain line),[28] Okuno (solid curve),[7] Vainstein *et al.* (dashed curve)[8] and Dettman *et al.* (dotted curve).[9]

In Fig. 7, published experimental results are also shown for comparison. We see that there are close agreements between the present values and the values reported by Okuno[7] and Dettman *et al.*[9] within the estimated errors. The agreements in Figs. 6 and 7 led us to conclude that the present experimental apparatuses for the partial and absolute total cross-section study can provide reliable results.

Figure 8 shows the absolute partial and total (apparent and counting) cross-sections of Eu atom. Each partial curve is an average of three to five independent runs. The partial cross-sections reported by Shimon *et al.*[10] are also shown for comparison.

We see in Fig. 8 that results of Shimon *et al.* do not agree with the present results in two points. First, the cross sections obtained by Shimon *et al.* are generally larger than those in the present study. Second, the energy dependence near threshold of each of their Eu^+ and Eu^{3+} curves differs from those in the present ones. A remarkable difference between the two results is the peak around 9 eV seen in the present Eu^+ curve. This peak was well reproduced in our measurement, and will be discussed in §4.3.

4.2 Uncertainties in the results on Ba and Eu atoms

The accuracy of the absolute total cross sections measured depends on how accurately the quantities in eqs. (4) and (6) can be determined. Table I summarizes the estimation of uncertainties in the present measurement. In the followings, we discuss the error sources and their uncertainties in each quantity in detail.

4.2.1 Electron current I_e

Main factors to be considered in correct measurement

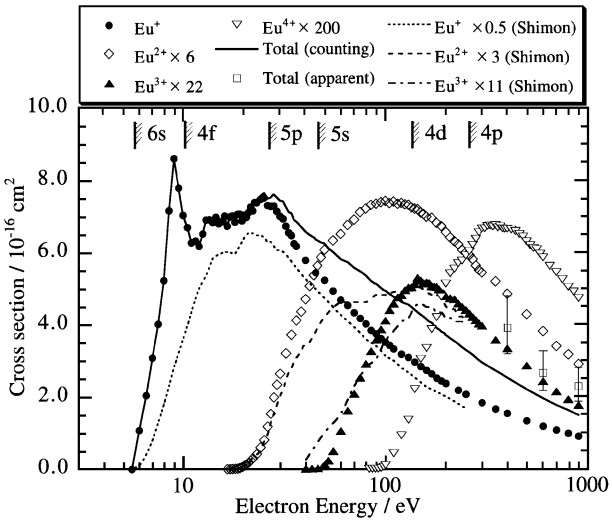

Fig. 8. The partial and absolute total cross-sections for ionization of Eu atom as a function of electron energy. The present cross sections σ_+, σ_{2+}, σ_{3+} and σ_{4+} are shown by symbols. The σ_{2+}, σ_{3+} and σ_{4+} curves are scaled up by 6, 22 and 200 times, respectively. The solid curve is the present counting cross section σ_c. Open squares indicate the present values of σ_T. Also the experimental results of σ_+, σ_{2+}, and σ_{3+} by Shimon *et al.* are shown by dotted, dashed and chain curves, respectively. Thse curves are illustrated by 1/2 scale of the present results. The vertical lines show threshold of each subshell electrons.

of I_e are secondary electrons from the electron-collector (EC) surface, scattering of ionizing electrons from the collector edges and target atoms, and electrometer used. In the present EC geometry, the leaving of secondary electrons might depend on the bias voltage on EC, the potential of EC with respect to that of the ionization section (0 V). The electron current I_e was therefore examined changing the bias voltage. For the electron energy of 400 eV, the electron current reached an equilibrium when the bias voltage was raised to +30 V. The bias voltage corresponding to electron energy 900 eV was +34 V. Consequently, the voltage on EC was kept at +35 V throughout the absolute measurement. As another check, I_e was monitored changing the field strength E_c applied in the ionization region to collect ions. When the electron energy was 400 eV, the current I_e started to decrease around $E_c = 30$ V/cm. The field strength $E_c = 15.0$ V/cm used in the measurement was such that it was sufficiently strong to collect ions efficiently but sufficiently weak not to deflect the electron beam appreciably. The fraction of electrons scattered out by elastic and inelastic collisions with target atoms and background molecules is estimated to be at most 10^{-4}. Thus uncertainty in the electron collection is due mainly to the scattering by the edges of the electron collector and is estimated to be ±2%. The electrometer used to measure I_e has a ±2% uncertainty. We estimate the entire uncertainty in the measurement of I_e to be ±4%.

4.2.2 Ion current I_i

It is necessary to ensure that the ions produced in the definite collision volume are collected accurately. Factors which might bring uncertainties into I_i are the thermal motion of target atoms, the scattering of product ions by the grid of ID and target atoms, electrometer used, and impurity ions.

A certain part of the target atoms have very high velocity, corresponding to the higher velocity tail of Maxwell-Boltzman distribution. Also some target atoms have diverging velocity components. Consequently, there is a possibility that a certain part of ions produced in the collision volume fail to enter the ion collector. We estimate the uncertainty caused by these effects to be 5%.

The geometrical transmission of the grids spanned over the opening of ID was 99.2%, and was taken into account in the calculation of the cross section. Scattering by and charge transfer neutralization in collision with target atoms are possibly negligibly small because the target-atom density is at most of the order of 10^{11} atoms/cm^3. Thus the uncertainty due to scattering comes mainly from scattering by the grid, and is estimated to be ±2%. The uncertainty of the electrometer used to measure I_i is ±2%. From the mass spectra recorded at the time of partial cross-section measurement, we estimate 5% uncertainty as arising from impurity ions. On the basis of these consideration, the entire uncertainty in the measurement of I_i is estimated to be ±14%.

4.2.3 Effective collision length L

We assumed that the effective collision length L is the same as the length of ID window, 5.8 mm, along the electron beam axis. This assumption becomes real if the electric-field E_c applied in the ionization region is uniform and if the orbit of the electron beam does not change. Unfortunately we could not confirm the field uniformity experimentally, so that the distribution of E_c in the ionization region was simulated by computer software "Shimion". The result showed that the E_c around the collision volume was satisfactorily uniform. On the other hand, the field E_c affects more or less the transmission of the electron beam, and makes L longer. A simple calculation shows that the increase in L due to the field of $E_c = 15$ V/cm is only 0.04% for 400 eV electrons. Consequently, the change in L due to the field E_c was not included in the calculation of σ_c. From these consideration, we estimate the uncertainty in the effective collision length L to be ±5%, as arising from the uncertainty in the geometrical scale of the ID window and from the field distortion.

4.2.4 Average ion charge $\langle q \rangle_{\rm av}$

The average charge $\langle q \rangle_{\rm av}$ was calculated using eq. (5) from the results of mass spectra recorded at electron energy 400 eV. Some error in $\langle q \rangle_{\rm av}$ might result from discrimination for ions with different charge in the measurement of mass spectra. The experimental uncertainty in $\langle q \rangle_{\rm av}$ is estimated to be ±3%.

4.2.5 Intensity ratio I_C/I_S

As has been described in §3.2, the intensity ratio I_C/I_S was determined directly with surface ionization detectors. The detector is composed of a 0.15 mm tungsten wire and an ion collector of condenser type. In this measurement, the tungsten wires of the detectors were positioned at the collision center and the quartz crystal sensor in the absolute measurement. The two surface ionization detectors were made in the same design and were operated under the same condition. After a number of measurements with different surface temperatures and atomic-beam intensities, and at an appropriate bias voltage between the tungsten wire and the ion collector, we obtained $I_C/I_S = 99.5$ within ±7% accuracy.

4.2.6 Accumulation coefficient η

The accumulation coefficient η (or sticking probability) is defined as the sticking probability of atoms that strike the sensor surface. Although the experimental determination of η is very difficult, and has not been done in the present work, some information about it is fortunately available. First, Okuno *et al.*[21] measured the coefficient η using a hollow cavity arrangement, and obtained $\eta = 0.95$ for Mg atom incident on a cold-trap surface with estimated accuracy of 5%. Second, Shibata and Ogura[22] have measured recently η values for Nd and Gd atoms incident on a quartz crystal sensor of the same type as in this study. They used an hollow cavity arrangement similar to that used by Vainshtein *et al.*[8] and obtained $\eta \fallingdotseq 1.00$. Third, in experiments where atomic beams of metallic elements are prepared using high-temperature ovens, we have obtained empirical evidence that reflection of atoms does not occur with an appreciable degree, even if the surface is at room temperature. Fourth, we examined once the effect of cooling of the quartz crystal sensor on the accumulation rate T. In this examination, we led first air at room temperature and then cold nitrogen gas from liquid nitrogen into the cooling pipe of the sensor. We observed no notice-

able change in T. Fifth, in the present case, the surface of the sensor faces directly the exit aperture of the oven. One possibility was then that the radiation from the oven might affect the sticking probability of atoms on the sensor surface. Consequently, before making the absolute measurement, we made performance tests of the quartz crystal sensor by vaporizing Ce which needs highest temperature among the elements we studied. The accumulation rate T on the crystal surface was monitored with the shutter opened and closed. When the shutter was closed the accumulation stopped without time delay, and did not change more. We concluded that the accumulation rate was not influenced by the heat from the oven. From these informative evidences, we assumed $\eta = 1$ with estimated uncertainty of 5%.

4.2.7 Accumulated mass $T \cdot \rho$

The measurement of T is based on the commercial quartz crystal sensor. According to its manual, the errors in the measurement of T is less than 5%. However, the accumulation rate T displayed on the controller panel of the sensor is calculated from the accumulated mass m per cm^2 and the tabulated density ρ of the substance in solid phase using the relation $T = m/\rho$. Because the uncertainty in T is based on that in the determination of mass m ($=T\cdot\rho$),[18] we need not to estimate uncertainties in T and ρ separately. On the basis of this result, we estimate the uncertainty in $T \cdot \rho$ to be $\pm 5\%$.

4.2.8 Average velocity $\langle\nu\rangle_{\rm av}$

In the determination of the average velocity $\langle\nu\rangle_{\rm av}$ of target atoms using TOF technique, we first calculated the average flight time $\langle t\rangle_{\rm av}$ from the time spectrum recorded in the storagescope. We, then, calculated the average velocity $\langle\nu\rangle_{\rm av}$ from $\langle t\rangle_{\rm av}$ and the effective flight length. The uncertainty in $\langle\nu\rangle_{\rm av}$, therefore, comes directly from those in $\langle t\rangle_{\rm av}$ and in the effective flight length. We estimate the uncertainty in $\langle t\rangle_{\rm av}$ to be $\pm 2\%$ as arising from the finite pulse width. The uncertainty in the effective flight length is estimated to be $\pm 3\%$. This uncertainty comes from the fact that the actual flight length differs depending on which point in the cone of the channeltron the ion hits. In addition to these two error sources, the statistical treatment in the calculation of $\langle t\rangle_{\rm av}$ gives rise to $\pm 5\%$ uncertainty. Thus the uncertainty in the determination of $\langle\nu\rangle_{\rm av}$ amounts to $\pm 10\%$.

4.2.9 Collision volume

There is an important factor which have not yet been considered as an error source. Equation (4) is based on the assumption that the collision volume is a cylinder of length L times the cross section S of the electron beam, and the target-atom density in the volume is uniform. In fact, however, the electron beam will diverge slightly, and will be distorted due to the field E_c. The estimated uncertainty attributed to these effect is $\pm 5\%$. As for the target uniformity, the deposited film accumulated on the surface of the cold trap indicated that the target-atom density N is sufficiently uniform in the collision region. Nevertheless, we estimate $\pm 3\%$ uncertainty as arising from the ununiformity of N.

Table I. Estimation of uncertainties for each quantity in eqs. (4) and (6).

	Uncertainties (in %)	Error sources considered
I_e Electron current	± 4	Scattering effect Electrometer used
I_i Ion current	± 14	Thermal motion of ions Scattering effect Electrometer used Impurity ions
L Effective collision length	± 5	Field distortion Change in L due to E_c Opening of the ion collector
$\langle q\rangle_{\rm av}$ Average charge	± 3	Discrimination effect
I_c/I_s Intensity ratio	± 7	Positions of the surface ionization detectors Difference in the surface ionization efficiency Electrometer used
η Accumulation coefficient	± 5	Scattering of atoms from the quartz sensor surface
$T \cdot \rho$ Accumulation rate	± 5	Quartz crystal sensor
$\langle\nu\rangle_{\rm av}$ Average velocity	± 10	Flight length Finite pulse width Evaluation of $\langle t\rangle_{\rm av}$
Collision volume	± 8	Distortion of assumed collision volume Target uniformity
Total uncertainty (quadrature sum)	± 22.6	

4.3 Discussion

The total systematic uncertainty (quadrature sum) in the present cross-section measurement is $\pm 23\%$. This is considerably larger than $\pm 3.5\%$ in the Ar^+ cross section obtained in the target gas-electron beam method[15] and ± 6–$\pm 12\%$ in the various cross sections obtained in the fast neutral beam method.[13,14] The present total uncertainty is dominated by those of the ion current I_i, the intensity ratio I_C/I_S and the average velocity $\langle\nu\rangle_{\rm av}$. These are, therefore, key factors in obtaining cross-section results with better accuracy. For example, determination of $\langle\nu\rangle_{\rm av}$ using the Doppler shift of resonance fluorescence excited by laser light incident on an atomic beam at an oblique angle would be promising for several atomic species.

Now, we discuss the ionization processes in collisions of electron with Eu atom. The ground state of Eu atom is [Xe]$4f^7 6s^2$ ($^8S_{7/2}$). The lowest state of the first excited $4f^7 5d6s$ configuration lies about 1.6 eV above the ground state. Consequently, at the evaporation temperature of about 1000 K, the population of excited target atoms are negligibly weak. The ionization thresholds of subshell electrons of the Eu atom based on photoelectron spectroscopy are indicated at the top of Fig. 8.

In the analysis of the experimental results, we assume as the basis of consideration that the cross section for direct ionization of an electron of individual subshell

varies smoothly; it increases from its ionization threshold, reaches the maximum at about three to four times the threshold value, and then decreases more slowly than the initial rise. This assumption is based on a number of previous experimental and theoretical studies on various atomic species, and is considered to be reasonable. This assumption then allows us to identify several interesting indirect processes.

First, the Eu^+ curve has a significant structure, and tells us the existence of certain indirect processes. According to the photoelectron spectrum on Eu atom reported by Richter *et al.*,[19] the ground $4f^76s$ $(^{7,9}S)$ state of Eu^+ ion formed by ionization of a $6s$ electron lies at 5.8 eV above the ground $4f^76s^2(^8S_{7/2})$ state of Eu atom. The $4f$-ionization states $Eu^+(4f^66s^2, {}^7F)$, $Eu^+(4f^66s^2, {}^5L)$ and $Eu^+(4f^66s^7s)$, lie at 10.3 eV, 15.4 eV and 17.5 eV, respectively, above the ground state of Eu atom (see Fig. 9). The former two states are lower than the appearance potential of Eu^{2+} ion, 16.9 eV. There is an unassigned Eu^+ state of $4f^66s^2$ configuration at 13.4 eV. It follows, then, that there are a number of $4f$-hole excited neutral states converging to these excited states, and most of these states can autoionize to form Eu^+ ion. The peak around 9 eV is probably attributed to the excitation of autoionizing $4f^66s^2$ (^7F) nl states. However, this peak is too sharp to be explained by the direct excitation of a $4f$ electron. One clue to this phenomenon is available in recent experimental studies of electron impact excitation of alkali atoms. Feuerestein *et al.*[23] observed a sharp near-threshold peak in the electron-impact excitation cross section of $K^{**}(3p^54s^2, {}^2P_{3/2})$ autoionizing state, and explained as due to negative-ion resonance. Borovik *et al.*[24] also observed several sharp peaks in the excitation function of metastable $K^{**}(3p^54snl, {}^4L_J)$ autoionizing states near the $3p$ excitation threshold. A similar near-threshold behavior has been observed in Li[25] and Na.[26] Thus, one possible explanation of the sharp peak around 9 eV in the Eu^+ cross-section curve is the resonance excitation of $4f^66s^2(^7F)nl$ autoionizing states via temporal formation of negative ion. Probably, one of the $4f^66s^2(^7F)nl$ states, which makes a weak attractive potential for the incident electron, is preferentially excited with a high probability. We can see also rather complex weak peak structure appearing in the 11–18 eV region. This structure may be attributed to resonance excitation of higher autoionizing $4f$-hole neutral states.

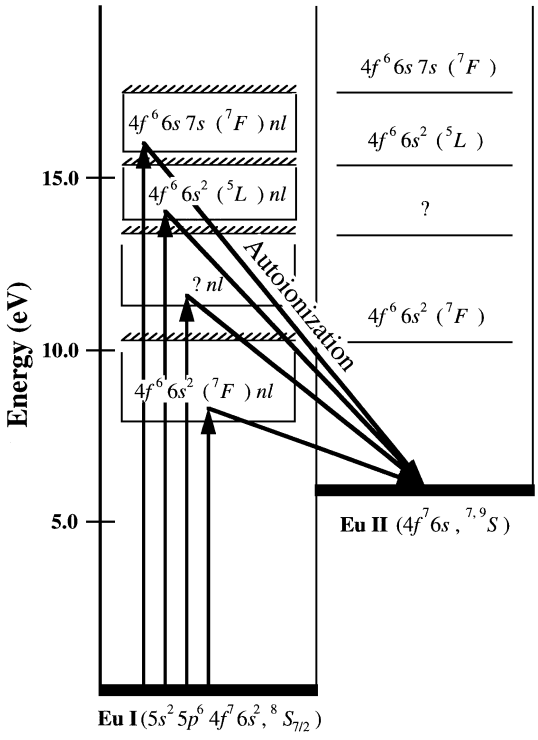

Fig. 9. Energy-level diagram of Eu atom. This is based on the photoelectron spectroscopic data of Richter *et al.*[19]

The Eu^{2+} curve is dominated by ionization of $5p$ electron. In the formation of Eu^{2+} ions, two ionization mechanisms are possible. One is direct double ionization in which the simultaneous ionization of two electrons occurs. Another is Auger process following the ionization of an inner subshell electron. The threshold of double ionization of Eu atom, 16.9 eV, is fairly below the ionization thresholds of $5p$ electron, 26.7 eV. Consequently, below the $5p$ ionization threshold, only the direct double ionization process can occur. In this case, we expect from the threshold law that the Eu^{2+} curve increases quadratically as a function of excess energy. The increase of the present Eu^{2+} curve near the threshold is approximately quadratic, in good agreement with this expectation. Above the $5p$ threshold, main role in the Eu^{2+} formation can be replaced by Auger process associated with the formation of $5p$-hole ionic states. According to the photoion-yield study of Dzionk *et al.*,[27] about 70% of the $5p$-hole states decays by Auger process to Eu^{2+} ion at about 4 eV above the $5p$ threshold.

Formation of triply charged Eu^{3+} ions, of which threshold is 41.8 eV, is very weak until the electron energy passes over the ionization threshold of $5s$ electrons (46.5 eV). Although the direct triple ionization of outer subshell ($5p$, $4f$, and $6s$) electrons can occur energetically below the $5s$ threshold, its probability is found to be extremely small. An appreciable formation of Eu^{3+} ions starts around the $5s$ threshold, indicating evidently that Eu^{3+} ions come from Auger process following the $5s$ ionizations.

The threshold for formation of Eu^{4+} ion is 84.4 eV. This energy is considerably lower than the ionization thresholds of $4d$ electrons (137.6 eV). It is easy to recognize that the formation mechanism of Eu^{4+} ions above the $4d$ threshold is due mainly to Auger process following the ionization of $4d$ electron. The weak rising above the ionization threshold (262 eV) of $4p$ electron evidently shows that the $4p$ ionization contributes to some extent to the formation of Eu^{4+} ions. It is noteworthy to point out that formation of Eu^{4+} ions amounts already to a considerable level at the $4d$ threshold. This is commonly seen in Sm and Yb atoms for which we made measurement of σ_{4+}. The energy range from the appearance potential 84.4 eV to the $4d$ ionization threshold 137.6 eV is so wide that we could not expect an important role of the direct processes in this whole range. It follows then

that some indirect processes play non-negligible roles; the most probable processes are shake-up and shake-off associated with $5s$ and $5p$ ionization followed by Auger processes.

§5. Conclusions

We have measured absolute partial and total cross sections for electron impact ionization of Ba and Eu atoms using traditional apparatus designs combined with the quartz crystal atomic-beam sensor and the TOF determination of atomic velocity. The Ba results is in good agreement with previously reported results within the experimental errors. We have found that the present apparatus can determine the ionization cross sections with experimental accuracy of $\pm 23\%$ for the elements which require temperatures up to 1200 K for vaporization.

Absolute measurements of ionization cross sections for atoms of metallic elements are normally time-consuming. One operation of the oven may provide formally only one determination at a given electron energy for a given atomic species. The present method using the quartz crystal sensor is apparently advantageous on this point; one operation of the oven allows us to determine the cross-section value several times at each of the given electron energies for a given atomic species.

The results of Eu atom have provided interesting and valuable information about the ionization processes. In particular, the Eu^+ cross section curve shows remarkable peak structure near the $4f$ ionization thresholds, which may be attributed to the resonance excitation of $4f^6 6s^2 nl$ autoionizing states via temporal negative ion formation.

Acknowledgement

We would like to express Dr. Takemasa Shibata of Japan Atomic Energy Research Institute for valuable discussion and comments.

The present work was partially supported by the Grant-in-Aid for Scientific Researches (07640537) from the Ministry of Education, Science, Sports and Culture.

1) L. J. Kieffer and G. H. Dunn: Rev. Mod. Phys. **38** (1966) 1.
2) T. D. Märk: Intern. J. Mass Spectros. Ion Phys. **45** (1982) 125.
3) H. Tawara and T. Kato: At. Data Nucl. Data Tables **36** (1987) 167.
4) H. Tawara and M. Kato: Research Report NIFS-DATA Series, NIFS-DATA-51 (1999).
5) E. W. McDaniel: *Atomic Collisions-Electron and Photon Projectiles* (Wiley, New York, 1989).
6) I. E. McCarthy and E. Weigold: *Electron-Atom Collisions* (Cambridge University Press, 1995).
7) Y. Okuno: J. Phys. Soc. Jpn. **31** (1971) 1189.
8) L. A. Vainshtein, V. I. Ochkur, V. I. Rakhovskii and A. M. Stepanov: Sov. Phys.-JETP. **34** (1972) 271.
9) J. M. Dettman and F. Karstensen: J. Phys. B **15** (1982)
10) L. L. Shimon, P. N. Volovich and M. M. Chiriban: Zh. Tekh. Fiz. **59** (1989) 64.
11) B. Sonntag and Zimmermann: Rep. Prog. Phys. **7** (1992) 911.
12) M. W. D. Mansfield: Giant Resonances in Atoms, Molecules, and Solids, ed. J. P. Connerade, J. M. Esteva and R. C. Karnatak (Plenum Press, New York, 1987) p. 91.
13) R. C. Wetzel, F. A. Baiocchi, T. R. Hayes and R. S. Freund: Phys. Rev. A **35** (1987) 559.
14) R. S. Freund, R. C. Wetzel, R. J. Shul and T. R. Hayes: Phys. Rev. A **41** (1990) 3575.
15) H. C. Straub, P. Renult, B. G. Lindsay, K. A. Smith and R. F. Stebbings: Phys. Rev. A **52** (1995) 1115.
16) K. J. Ross and B. Sonntag: Rev. Sci. Instrum. **66** (1995) 4409.
17) S. Okudaira: J. Phys. Soc. Jpn. **29** (1970) 409.
18) C. Lu: J. Vac. Sci. Technol. **12** (1975) 578.
19) M. Richter, M. Meyer, M. Pahler, E. Prescher, E. V. Raven, B. Sonntag and H. E. Wetzel: Phys. Rev. A **40** (1989) 7007.
20) R. D. Cowan: *The Theory of Atomic Structure and Spectra* (University of California Press, Berkeley, 1981).
21) Y. Okuno, K. Okuno, Y. Kaneko and I. Kanomata: J. Phys. Soc. Jpn. **29** (1970) 164.
22) T. Shibata and K. Ogura: private communication.
23) B. Feuerstein, A. N. Grum-Grzhimailo and W. Mehlhorn: J. Phys. B: At. Mol. Opt. Phys. **32** (1999) 4547.
24) A. A. Borovik, H. L. Rojas, G. C. King and E. Yu Remeta: J. Phys. B **32** (1999) 4225.
25) A. A. Borovik and V. N. Krasilinec: J. Phys. B **32** (1999) 1941.
26) B. Feuerstein, A. N. Grum-Grzhimailo and W. Mehlhorn: J. Phys. B: At. Mol. Opt. Phys. **31** (1998) 593.
27) C. Dzionk, W. Fielder, M. von Luck and P. Zimmermann: Phys. Rev. A **39** (1989) 1780.
28) R. H. McFaland: Phys. Rev. **159** (1967) 20.